

Geophysical Research Letters[®]

RESEARCH LETTER

10.1029/2022GL102055

Key Points:

- Revised implementation of noble gases in Bern3D model tuned to observations of saturation anomalies
- Complex interplay between air-sea gas exchange, overturning circulation, and noble gas saturation
- Including saturation effects noble gas-based mean ocean temperature of the last glacial maximum is 2°C colder than the Holocene

Supporting Information:

Supporting Information may be found in the online version of this article.

Correspondence to:

F. Pöppelmeier,
frek.poeppelmeier@unibe.ch

Citation:

Pöppelmeier, F., Baggenstos, D., Grimmer, M., Liu, Z., Schmitt, J., Fischer, H., & Stocker, T. F. (2023). The effect of past saturation changes on noble gas reconstructions of mean ocean temperature. *Geophysical Research Letters*, 50, e2022GL102055. <https://doi.org/10.1029/2022GL102055>

Received 7 NOV 2022
Accepted 13 MAR 2023

© 2023 The Authors.

This is an open access article under the terms of the [Creative Commons Attribution-NonCommercial License](https://creativecommons.org/licenses/by-nc/4.0/), which permits use, distribution and reproduction in any medium, provided the original work is properly cited and is not used for commercial purposes.

The Effect of Past Saturation Changes on Noble Gas Reconstructions of Mean Ocean Temperature

Frerk Pöppelmeier^{1,2} , Daniel Baggenstos^{1,2,3} , Markus Grimmer^{1,2}, Zhijun Liu^{1,2,4} , Jochen Schmitt^{1,2} , Hubertus Fischer^{1,2} , and Thomas F. Stocker^{1,2} 

¹Climate and Environmental Physics, Physics Institute, University of Bern, Bern, Switzerland, ²Oeschger Centre for Climate Change Research, University of Bern, Bern, Switzerland, ³Australian Antarctic Division, Kingston, TAS, Australia, ⁴GFZ German Research Centre for Geosciences, Potsdam, Germany

Abstract The ocean's immense ability to store and release heat on centennial to millennial time scales modulates the impacts of climate perturbations. To gain a better understanding of past variations in mean ocean temperature (MOT), a noble gas-based proxy measured from ancient air in ice cores has been developed. Here we assess non-temperature effects that may influence the atmospheric noble gas ratios reconstructed from polar ice and how they impact the temperature signal with an intermediate complexity Earth system model. We find that changes in wind speed, sea-ice extent, and ocean circulation have partially compensating effects on mean-ocean noble gas saturation, leading to a slight reduction of noble gas undersaturation at the Last Glacial Maximum (LGM). Taking these effects and ice core measurements into account, our model suggests a revised MOT difference between the LGM and pre-industrial of $-2.1 \pm 0.7^\circ\text{C}$ that is also in improved agreement with other independent temperature reconstructions.

Plain Language Summary Most of the heat added to the climate system by anthropogenic climate change is taken up by the oceans. To better understand how the ocean responds to climate change over hundreds to thousands of years, an indirect measure for the mean ocean temperature (MOT) based on the temperature-dependent solubility of noble gases has been developed. Noble gas concentrations of the past atmosphere are archived in air bubbles in polar ice cores, which have been used to reconstruct the MOT of the past 20,000 years when Earth's climate was propelled out of the last ice age. However, uncertainties remain regarding critical parameters that are required to derive the correct MOT of the past. Here we make use of an Earth system model that explicitly simulates the noble gases and allows us to assess these parameters in detail under modern and past climate conditions. We find that changes in wind, sea-ice, and ocean circulation all play important roles in the partitioning of noble gases between the atmosphere and ocean. By taking these effects into account our model suggests a revised best-estimate MOT cooling of the last ice age to $-2.1 \pm 0.7^\circ\text{C}$, which is about 0.5°C warmer than previous estimates.

1. Introduction

The global ocean plays a critical role in regulating Earth's climate due to its large heat capacity and inter-hemispheric heat transport by the global overturning circulation (Stocker, 2000). Yet, constraining changes in ocean heat content and thus Mean Ocean Temperature (MOT) is notoriously difficult with in situ measurements alone due to their spatio-temporal limitations. Great progress has been made for today's ocean through the deployment of vast fleets of Argo floats (Gleckler et al., 2016), but reconstruction of past MOT from in situ deep sea sediments remains very challenging. At the same time the large swings in Earth's past climate hold the potential to inform us about mechanisms and feedbacks that are crucial for a better understanding of the ongoing anthropogenic climate change. To remedy this shortcoming a MOT proxy has been developed using polar ice cores that is founded in the temperature-dependent solubilities of quasi-inert gases, which partition their globally conserved inventories between the atmosphere and ocean on orbital to millennial time scales (Headly & Severinghaus, 2007). These gases include the heavy noble gases krypton (Kr) and xenon (Xe) as well as nitrogen (N_2), which we hereafter refer to as noble gases, noting that N_2 is conserved over glacial-interglacial time scales. The solubilities of the noble gases increase with colder temperatures, and the extent thereof increases with atomic weight, such that Xe is more sensitive to temperature variations than Kr, and Kr more sensitive than N_2 . The atmospheric ratios of Kr and Xe relative to N_2 (in δ -notation relative to the modern atmosphere, $\delta\text{Kr}/\text{N}_2$ and $\delta\text{Xe}/\text{N}_2$) decrease for a colder ocean, because the relative changes of dissolved Kr and Xe are larger than for N_2 . The amount of noble gases in

any water parcel in the ocean is set at the time it has last been at the ocean surface and exchanged with the atmospheric noble gases at its surface temperature at that time. Thus, atmospheric noble gas ratios, archived in polar ice, can be used to infer MOT. Through analytical advancements in measuring atmospheric noble gas concentrations and their isotopic composition, past MOT variations have been reconstructed from various time periods with remarkable precision (Baggenstos et al., 2019; Bereiter, Shackleton, et al., 2018; Haeberli et al., 2021; Shackleton et al., 2019, 2020, 2021).

However, critical uncertainties persist that are associated with post-coring gas loss and firn fractionation corrections (Haeberli et al., 2021), and systematic uncertainties in the inference of MOT from paleo-atmospheric noble gas ratios (Bereiter, Shackleton, et al., 2018; Ritz, Stocker, & Severinghaus, 2011). For the latter, previous studies employed a simple box model, which requires a number of only poorly constrained input parameters and that also does not form a physically consistent framework with regard to mixing processes and oceanographic parameters (Bereiter, Kawamura, & Severinghaus, 2018). A key parameter for the assessment of past MOT from noble gases is their saturation state. In the modern ocean the heavy noble gases are undersaturated below about 1 km water depth (Hamme et al., 2019). This undersaturation is the result of a number of processes. First, rapid sea surface cooling at high-latitudes and subsequent deep convection keeps noble gases from fully equilibrating (Hamme & Severinghaus, 2007; Hamme et al., 2017; Seltzer et al., 2019). Second, sea-ice cover restricts air-sea gas exchange while heat is still transported through the ice (albeit at a relatively slow rate compared to the open ocean). And third, subsurface melting of glaciers, which requires large amounts of latent heat and thus lowering ocean temperature independent of air-sea gas exchange (Loose et al., 2016). Further parameters that influence the solubility and hence saturation are wind speed and ocean circulation, but also the relative contributions of water masses and their properties (i.e., temperature and salinity), which may have different saturation levels. For previous assessments of past MOT, this undersaturation was often assumed temporally constant due to a lack of constraints (Haeberli et al., 2021; Shackleton et al., 2020). Here we note the saturation anomaly as $\Delta X = [X]_m/[X]_{eq} - 1$ (%), where $[X]_m$ and $[X]_{eq}$ are the simulated/measured and equilibrium concentrations of gas X.

In this study, we use the Bern3D Earth system model of intermediate complexity that is equipped with noble gas tracers to explore the impact of temporally variable global mean saturation on the atmospheric noble gas ratios archived in polar ice cores and how this influences the inference of MOT. With this physically consistent framework we then assess biases in the previously used noble gas-MOT box model, and provide new constraints on the difference in MOT between the Last Glacial Maximum (LGM) and pre-industrial (PI) taking into account changes in saturation. We infer systematic effects of various processes on the noble gas ratios of the past atmosphere, acknowledging that the size of the derived effects may be model-dependent.

2. Model and Experiments

2.1. Bern3D Model

The Bern3D model (v2.0) is an intermediate complexity Earth system model with a geostrophic-frictional ocean on an irregular 41×40 grid with 32 logarithmically scaled vertical layers including an isopycnal diffusion scheme and a Gent-McWilliams parameterization of eddy-induced transport (Müller et al., 2006). It is coupled to a thermodynamic sea-ice module and a simple two-dimensional energy-moisture balance model of the atmosphere (Ritz, Stocker, & Joos, 2011) on the same horizontal grid. The noble gas and N_2 implementations are described in detail in Ritz, Stocker, and Severinghaus (2011). Air-sea gas exchange is calculated as

$$F_{as} = k(C_{sat} - C) \quad (1)$$

with C_{sat} the saturation concentration, C the surface concentration, and k the gas transfer velocity, which depends on fractional sea-ice cover, surface wind speed, and Schmidt number as described in detail by Müller et al. (2008). The temperature and salinity-dependent solubility functions have been updated here with the empirical relationships by Jenkins et al. (2019) which provide consistent formulations for all noble gases. Wind stress and wind speed are prescribed from monthly climatologies (Kalnay et al., 1996). Bubble injection is not considered here. Sea surface pressure is assumed globally uniform and changes from the present day are taken into account offline.

In order to tune and validate the noble gas implementations in the model against observations, we calculate the saturation anomalies based on the three-dimensional potential temperature and salinity fields provided by the model and compare these to the compilation by Hamme et al. (2019) (Figure 1a). For better consistency

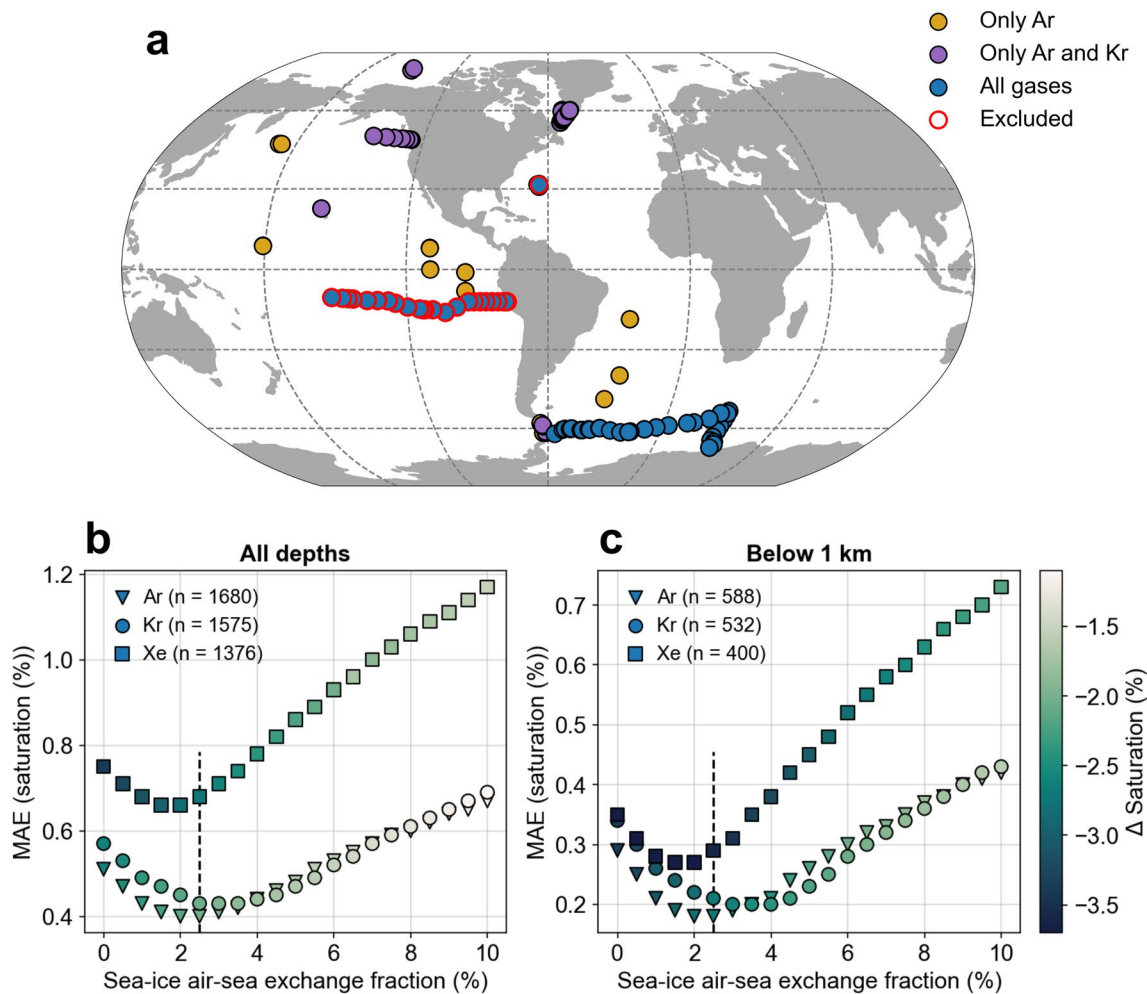


Figure 1. (a) Map with seawater stations for which noble gas concentrations were measured as compiled by Hamme et al. (2019). Red circles mark stations that were excluded for the tuning of the model, as inter-laboratory comparisons suggest unreliable data for these stations (Hamme et al., 2019). (b) Fraction of air-sea gas exchange under sea-ice versus cost function (Mean Absolute Error) for all depths and (c) for depths below 1 km. Vertical dashed line marks the combined minimum of the cost function of all three noble gases.

we re-calculate the saturation anomalies of Hamme et al. (2019) with the solubility formulations of Jenkins et al. (2019). In the standard model setup, air-sea gas exchange under sea-ice is completely prohibited, which leads to substantial undersaturation of the noble gases in the model. To achieve a better model-data agreement, we tune the fraction of air-sea gas exchange under sea-ice by varying it between 0% and 10% of the gas exchange that would take place without sea-ice. This small air-sea gas exchange under the sea-ice can be understood as the effect of leads and small polynyas that are not resolved in the model. Even though argon (Ar) cannot be used to constrain MOT from ice cores due to potential fractionation processes during bubble enclosure, we make use of this tracer for the tuning as its undersaturation in the ocean is determined by the same processes that impact Kr and Xe saturation. At the same time, the data-coverage is even better for Ar than for Kr and Xe.

2.2. Sensitivity Experiments and LGM Simulations

To explore the response of atmospheric $\delta\text{Kr}/\text{N}_2$ and $\delta\text{Xe}/\text{N}_2$ to external forcing that impacts MOT and/or the ocean circulation, we conducted a number of sensitivity experiments. First, we performed three different simulations with radiative forcings equivalent to 0.5, 2.0, and 4.0 times PI CO_2 (equilibrium climate sensitivity of the model is 3.0°C) with all other boundary conditions as in the PI control.

Second, we investigated the response of the noble gases to the colder climate of the LGM. The applied boundary conditions for the LGM are described in detail by Pöppelmeier et al. (2021) and include changes in orbital and

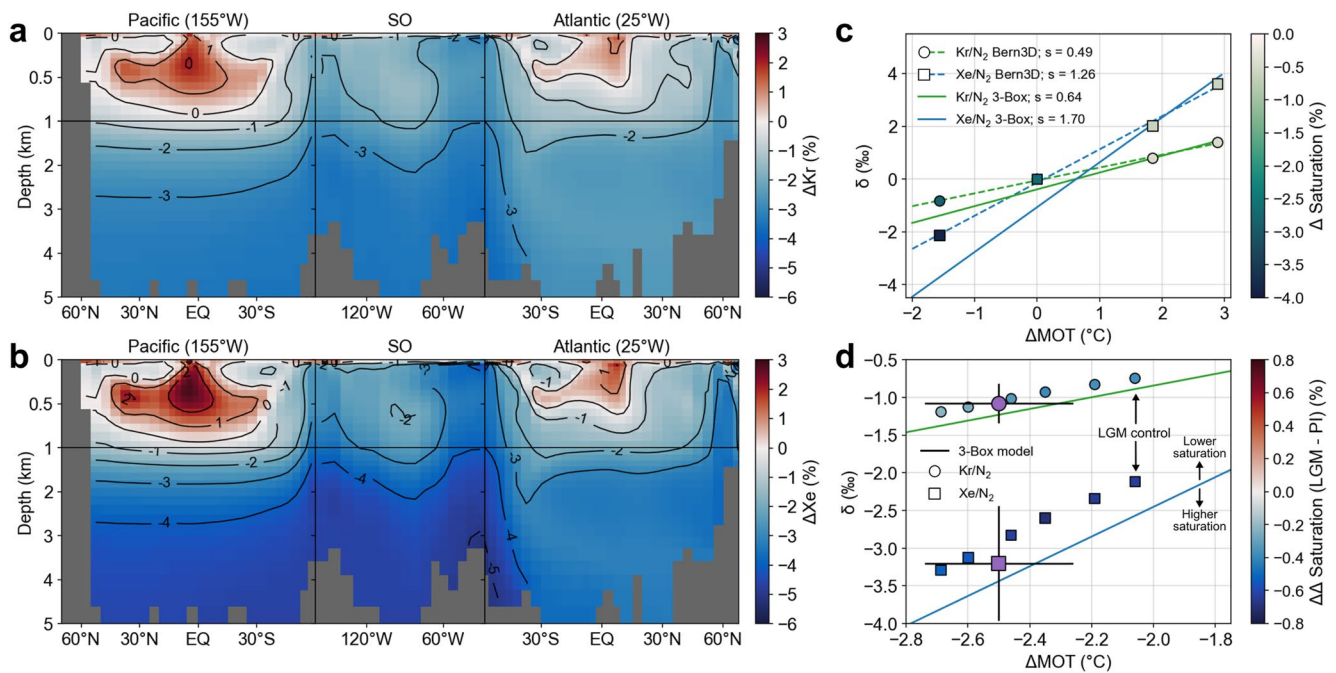


Figure 2. Global section of saturation anomaly of the pre-industrial control (PI) of (a) krypton and (b) xenon. (c) Sensitivity of $\delta\text{Kr}/\text{N}_2$ (circles) and $\delta\text{Xe}/\text{N}_2$ (squares) to changes in mean ocean temperature (MOT) induced by changing the radiative forcing of CO_2 , and associated global mean saturation of Kr and Xe (fill color) of the Bern3D (dashed) and 3-box model (solid). The slopes of the fits are denoted in the legend in units of $\%/^\circ\text{C}$. All δ -values are plotted relative to the PI control simulation of Bern3D. (d) MOT anomaly versus $\delta\text{Kr}/\text{N}_2$ and $\delta\text{Xe}/\text{N}_2$ of Bern3D Last Glacial Maximum simulations (Methods), the idealized 3-Box model (lines) and the ice core reconstruction by Bereiter, Shackleton, et al. (2018) (purple). Deviations from the idealized 3-Box model are caused by different saturation concentrations.

albedo forcing, greenhouse gases, aerosol radiative forcing, a closed Bering Strait, wind stress and speed, and vertical mixing due to changes in tidal dissipation induced by the lower sea-level. The glacial Atlantic Meridional Overturning Circulation was forced by freshwater correction fluxes to a strength of 11.5 Sv (relative to 17.7 Sv at PI). To assess the impact of even colder temperatures on the noble gases, we performed further experiments with additional top-of-the-atmosphere radiative forcing between -0.5 and -1.5 W/m^2 . The effect of different saturation anomalies on the atmospheric noble gas ratios under LGM boundary conditions was investigated by changing the residual air-sea gas exchange under sea-ice (as for the tuning of the PI state) in sensitivity experiments. All simulations were run for 10 kyr to ensure that they reached steady-state.

3. Results and Discussion

In order to establish the correct $\delta\text{Kr}/\text{N}_2$ and $\delta\text{Xe}/\text{N}_2$ to MOT relationships in the model, it is imperative to accurately simulate the dissolved Kr, Xe, and N_2 concentrations. However, not all processes that are thought to play a role in setting the noble gas saturation anomalies are implemented in the Bern3D model (i.e., bubble injection and subsurface glacial melt water are missing), and we here therefore follow a more idealized approach. We note that these simplifications may cause our results to be model dependent, but they are informative nonetheless and should form the basis for future investigations that explicitly include these processes.

We only tune the fraction of air-sea gas exchange allowed through sea-ice to achieve a better model-data agreement in terms of noble gas saturation anomalies (here Ar, Kr, and Xe). The minima of the cost-function (Mean Absolute Error) range between 1.5% and 3.5% air-sea gas exchange under sea-ice depending on the noble gas (Figures 1b and 1c), but independent of the considered depth (i.e., all depths or for depths below 1 km). Since there does not appear to be a systematic bias in the location of the minimum dependent on the choice of noble gas, we simply choose the average of the three minima, that is, 2.5% air-sea gas exchange through sea-ice, for the subsequent simulations (see Figures 2a and 2b for spatial distributions of saturation anomalies). Yet, we stress that this cannot be seen as a constraint for the true air-sea gas exchange through sea-ice due to the reduced complexity of the employed sea-ice model, and instead should be solely considered as a tuning parameter.

3.1. Sensitivities to External Forcings

Previously, Ritz, Stocker, and Severinghaus (2011) performed sensitivity experiments with the Bern3D model (v1.0) to assess the impacts of various parameter choices and external forcings on the $\delta\text{Kr}/\text{N}_2$ -MOT relationship. Since we here employ a different model version with a different resolution, revised atmospheric, ocean, and sea-ice parameters, changed noble gas solubility parameterization, and tuned the model to better represent modern noble gas undersaturation, we performed similar experiments to briefly re-evaluate these impacts in the revised model framework. As such, we are able to highlight the impacts these model changes have on the noble gas response to climate and ocean perturbations and thus better assess gaps of knowledge in the understanding of atmospheric noble gas ratios.

The major difference between the present and the earlier study with regard to noble gases is the allowed air-sea gas exchange under sea-ice, which was completely prohibited in Ritz, Stocker, and Severinghaus (2011). This notably reduces the amount of undersaturation under different climate states and thus directly impacts the $\delta\text{Kr}/\text{N}_2$ and $\delta\text{Xe}/\text{N}_2$ to MOT relationships (Figure 2a). Even though only a small fraction of air-sea gas exchange is allowed under sea-ice, its impact is important as it limits the undersaturation in colder climate states when sea-ice area is strongly expanded. Over a range of $\Delta\text{MOT} \approx 4.5^\circ\text{C}$ (between coldest and warmest sensitivity experiment) the global mean saturation anomalies vary by about 2.4% and 3.3% for Kr and Xe, respectively, which is mostly driven by a rapid decline in Southern Ocean sea-ice extent under warmer than modern climate states in the Bern3D model.

The influence of these changes in undersaturation on the sensitivity of the noble gases to changes in MOT can be assessed by comparing the $(\delta\text{Kr}/\text{N}_2)/\Delta\text{MOT}$ (and $(\delta\text{Xe}/\text{N}_2)/\Delta\text{MOT}$) slope to a simplified 3-box model for which constant global mean saturation anomalies of zero are assumed. In contrast to Bereiter, Shackleton, et al. (2018), we use temperature and salinity of three different water masses as simulated by different dye tracers in the Bern3D model (see Figure S1 in Supporting Information S1 for source regions). With this choice, the input parameters of the 3-box model directly correspond to the water mass properties in Bern3D, which allows for a direct comparison between both models. For the box model the slopes are $(\delta\text{Kr}/\text{N}_2)/\Delta\text{MOT} = 0.64 \text{ ‰}/^\circ\text{C}$ and $(\delta\text{Xe}/\text{N}_2)/\Delta\text{MOT} = 1.70 \text{ ‰}/^\circ\text{C}$, while we find for the Bern3D 0.49 and 1.26 $\text{‰}/^\circ\text{C}$, respectively (Figure 2c). This implies that a 1% change in global mean saturation anomaly (in absolute terms) of Kr and Xe causes offsets of 0.28 and 0.59 ‰ for $\delta\text{Kr}/\text{N}_2$ and $\delta\text{Xe}/\text{N}_2$, respectively, which corresponds to significant MOT biases of about 0.42 and 0.35 $^\circ\text{C}$, respectively (see Text S1 in Supporting Information S1 for details).

3.2. Simulated Noble Gases and MOT at the LGM

The climate state of the LGM was characterized by substantially colder temperature than modern, primarily caused by reduced greenhouse gas concentrations and increased albedo (Köhler et al., 2017). While the extent of Global Mean Surface Temperature cooling remains debated, recent studies appear to converge to LGM ΔGMST s between -4.5 and -7.1°C (Annan et al., 2022; Osman et al., 2021; Tierney et al., 2020) that are markedly colder than previous assessments (Annan & Hargreaves, 2013; MARGO Project Members, 2009). Reconstructions of MOT, based on the noble gas thermometry, first indicated a cooling of $-2.7 \pm 0.6^\circ\text{C}$ (Headly & Severinghaus, 2007) with tighter constraints of $-2.6 \pm 0.24^\circ\text{C}$ later provided by Bereiter, Shackleton, et al. (2018), $-2.7 \pm 0.4^\circ\text{C}$ by Baggenstos et al. (2019) and $-3.0 \pm 0.4^\circ\text{C}$ by Haerberli et al. (2021).

Yet, as a note of caution, these MOT anomalies were not calculated consistently between studies with some studies computing it relative to the early Holocene (Bereiter, Shackleton, et al., 2018), while other studies used the late Holocene (Baggenstos et al., 2019) or mean Holocene as reference (Haerberli et al., 2021). Here we compare LGM against PI steady-state simulations, and we therefore re-calculated the reconstructed noble gas-based MOT anomalies relative to the average of the late Holocene (0–4 kyr BP), which facilitates better comparability to other climate and ocean proxies. These LGM minus late Holocene MOT anomalies are slightly smaller than the values provided previously (Bereiter, Shackleton, et al., 2018; Haerberli et al., 2021; Headly & Severinghaus, 2007). Moreover, a mistake in the krypton inventory of the Bereiter, Shackleton, et al. (2018) box model was identified (Baggenstos, personal communication), which led to a discrepancy between the ΔMOT estimates from the different noble gas ratios. In response to that, Bereiter, Shackleton et al. (2018) adjusted the undersaturation such that the ΔMOT estimates were aligned again. To remedy this issue and to facilitate comparability to other model and ice core data, we re-calculated the MOT anomalies based on the Bereiter, Shackleton, et al. (2018)

paleo-atmospheric elemental ratios with the corrected box model (Table S1 in Supporting Information S1). For this, all parameters remained unchanged except for the solubility functions, which were updated to the formulation by Jenkins et al. (2019), and temporally constant undersaturation were assumed as by Baggenstos et al. (2019) and Haeblerli et al. (2021). Due to the compensating effects of the box model issue and adjusted undersaturation in Bereiter, Shackleton, et al. (2018), the re-calculated MOT LGM-PI anomaly of 2.51°C is virtually unchanged from the initial value provided by Bereiter, Shackleton, et al. (2018).

Our LGM control simulation exhibits a ΔGMST of -5.9°C in good agreement with previous studies (Tierney et al., 2020), but ΔMOT of only -2.1°C , which is 0.5°C warmer than suggested by the noble gas thermometry reconstruction by Bereiter, Shackleton, et al. (2018). At the LGM, atmospheric $\delta\text{Kr}/\text{N}_2$ is not only affected by changes in MOT, but the lower sea-level stand exerted additional indirect influences. The displaced water from the ocean to the continental ice-sheets in the form of freshwater caused the mean ocean salinity to increase by about 1.2 PSU, which also affected noble gas solubilities (Jenkins et al., 2019). Further, the ~ 130 m lower sea-level reduced the total ocean volume by about 3.5% (Lambeck et al., 2014) thereby diminishing its capacity to hold dissolved gases by an equivalent amount. Finally, the lower sea-level raised the sea-surface pressure by about 1.7%, which after Henry's law translates to an increase in the oceanic noble gas inventories also by $\sim 1.7\%$ (Headly & Severinghaus, 2007) (see Ritz, Stocker, and Severinghaus (2011) for individual attribution of the corrections on the noble gas ratios). With these additional effects taken into account, we simulate $\delta\text{Kr}/\text{N}_2$ and $\delta\text{Xe}/\text{N}_2$ values of -0.75 and -2.12 ‰, respectively, in the LGM control (relative to the PI, Figure 2d). We can again compare these results to the simple 3-box model, which yields $\delta\text{Kr}/\text{N}_2 = -0.89$ ‰ and $\delta\text{Xe}/\text{N}_2 = -2.57$ ‰ also considering the above-mentioned effects associated with the lower sea-level stand. These differences between Bern3D and the 3-box model indicate that the noble gas saturation anomalies must have changed for Bern3D between PI and LGM. Indeed, at the LGM the undersaturation is larger by 0.4% and 0.6% for Kr and Xe ($\Delta\text{Kr} = -2.4\%$ and $\Delta\text{Xe} = -3.4\%$ at the LGM), respectively. Due to this increased undersaturation less Kr and Xe are dissolved in the ocean compared to the 3-box model that assumes constant undersaturation and atmospheric ratios are hence higher (Figure 2d). Note, that changes in N_2 saturation are simulated as well and are taken into account, but have negligible impact because of the substantially larger atmospheric reservoir of N_2 and lower sensitivity on its solubility on temperature compared to Kr and Xe.

Next to overturning circulation and sea-ice an additional process is important at the LGM in determining the change in noble gas saturation anomalies relative to PI. The massive continental ice-sheets caused average surface wind speeds at the northern high-latitudes to increase (Muglia & Schmittner, 2015) (see Figure S4 in Supporting Information S1 and Pöppelmeier et al. (2021) for details on the implementation), which also increases gas transfer velocities in the model. Decreasing saturation due to larger sea-ice extent (Figures S2 and S3 in Supporting Information S1) and increasing saturation as a result of a more sluggish ocean circulation and increased gas transfer velocities can partly compensate. In the LGM control run, however, this balance is in favor of the increased sea-ice extent. Consequently, the greater undersaturation of the LGM relative to the PI run increases the simulated glacial Kr/N_2 and Xe/N_2 ratios of the atmosphere, which contributes to the mismatch with reconstructed noble gas ratios ($\delta\text{Kr}/\text{N}_2 = -0.75$ vs. -1.08 ‰). This suggests that MOT must have been even colder than simulated here for the LGM to resolve the mismatch (Figure 3a). Sensitivity tests with additional negative radiative forcing indicate that a further MOT cooling of about 0.5°C is required in the model to reproduce measured $\delta\text{Kr}/\text{N}_2$ and $\delta\text{Xe}/\text{N}_2$ under LGM conditions. These simulations, however, then exhibit considerably larger ΔGMST s of around -8°C and global mean sea-surface temperature anomalies (ΔGSST) of up to -5°C that are greater than any temperature change inferred from previous reconstructions (see Tierney et al., 2020). While we acknowledge that $\Delta\text{GMST}-\Delta\text{MOT}$ and $\Delta\text{GSST}-\Delta\text{MOT}$ relationships are model dependent, their correlations in the Bern3D model fall in line with more complex models of the Paleo Model Intercomparison Project 3 (Bereiter, Shackleton, et al., 2018).

Then how can the discrepancy between simulated and reconstructed noble gas ratios be resolved? At this point, a systematic noble gas measurement bias seems unlikely, as the result was now reproduced by different laboratories and measured in three different ice cores (Baggenstos et al., 2019; Bereiter, Shackleton, et al., 2018; Headly & Severinghaus, 2007). Instead, the largest unknown remains the noble gas undersaturation in the past, which holds the potential to shift the inferred MOT in either direction.

In order to obtain a constraint on the smallest possible MOT cooling at the LGM, we performed an experiment with doubled gas transfer velocity and allowed for full gas exchange through sea-ice. Any undersaturation is

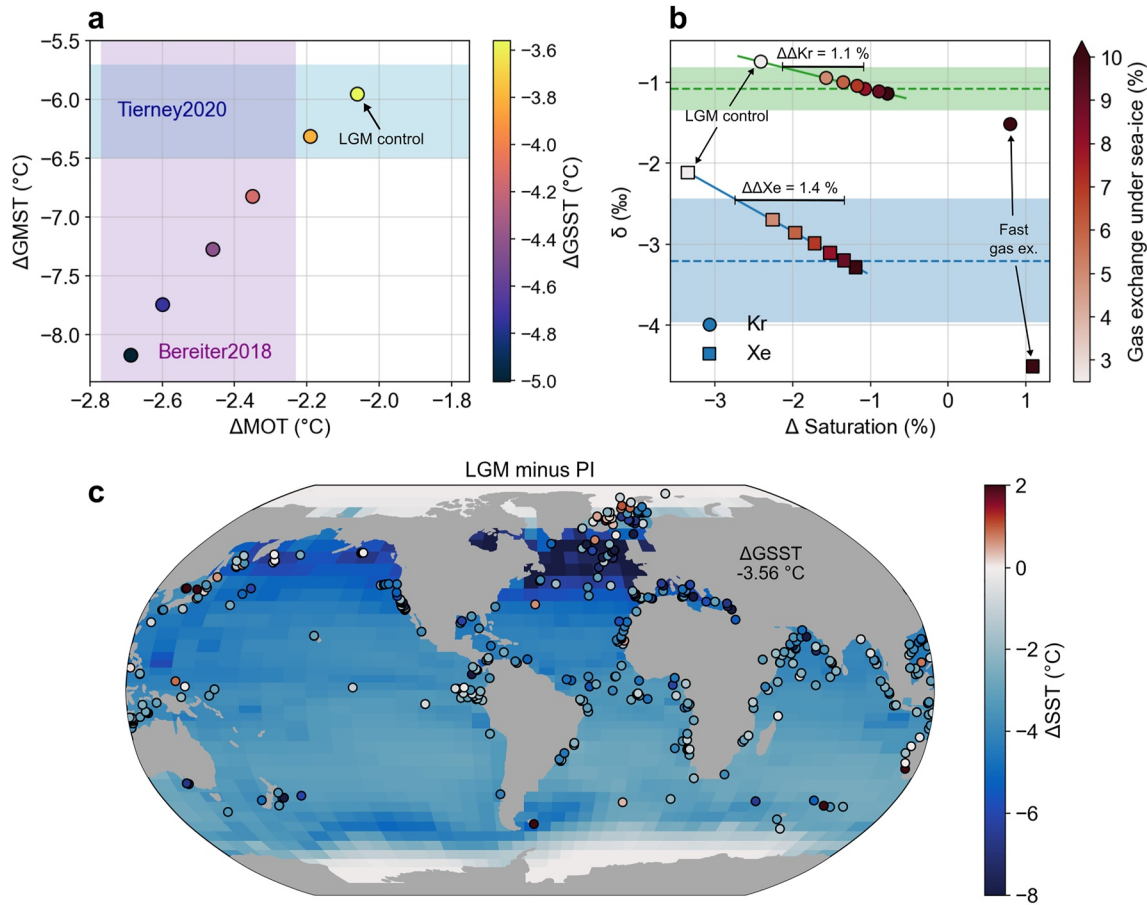


Figure 3. (a) Mean ocean temperature (MOT) anomalies versus Global Mean Surface Temperature (GMST) anomalies of the Last Glacial Maximum (LGM) simulations performed in this study. Estimates for ΔGMST and ΔMOT by Tierney et al. (2020) and Bereiter, Shackleton, et al. (2018) are marked as blue and purple shadings, respectively. (b) Saturation anomaly of Kr (circles) and Xe (squares) versus their atmospheric ratio for LGM simulations with different fractions of air-sea gas exchange allowed under sea-ice. Green and blue horizontal dashed lines and shadings depict measured $\delta\text{Kr}/\text{N}_2$ and $\delta\text{Xe}/\text{N}_2$ with their uncertainty, respectively (Bereiter, Kawamura, & Severinghaus, 2018). Solid green and blue lines mark linear fits through the data points which are used to translate the noble gas ratio measurement uncertainties into the uncertainties of the undersaturation. These are then converted to MOT uncertainties via the relationships derived from the sensitivity tests in Section 3.1 and yield $\pm 0.57^{\circ}\text{C}$ and $\pm 0.67^{\circ}\text{C}$ for Kr and Xe, respectively. (c) Sea surface temperature anomalies of the LGM control run with geochemical reconstructions compiled by Tierney et al. (2020) superimposed as filled circles.

then virtually eliminated, and mixing-induced oversaturation (see Hamme et al., 2019) becomes dominant in the entire ocean, with positive global mean saturation anomalies of $\Delta\text{Kr} = +0.8\%$ and $\Delta\text{Xe} = +1.1\%$ for Kr and Xe, respectively. Accordingly, this yields substantially lower atmospheric noble gas ratios of $\delta\text{Kr}/\text{N}_2 = -1.52\text{‰}$ and $\delta\text{Xe}/\text{N}_2 = -4.51\text{‰}$ (Figure S4 in Supporting Information S1) for ΔMOT of 2.1°C of the LGM control (Figure 3b). Using the noble gas ratio to ΔMOT relationships derived in Section 3.1, we can thus determine the minimum MOT anomaly of the LGM ice core measurements, which are -1.41°C for Kr and -1.33°C for Xe (i.e., differences of 0.69 and 0.77°C relative to the LGM control).

Importantly, the effect of different saturation anomalies produces also different ΔMOT offsets for Kr and Xe. This is also observed for reconstructed noble gases for two different ice cores (arguing against a local effect), which, translated to ΔMOT under the assumption of constant undersaturation, also give different temperature estimates that are colder by 0.3°C for $\delta\text{Xe}/\text{N}_2$ compared to $\delta\text{Kr}/\text{N}_2$ (Bereiter, Shackleton, et al., 2018; Haerberli et al., 2021). From this follows that the difference in LGM undersaturation between Kr and Xe was smaller than during PI, which can only be achieved with smaller saturation anomalies compared to the modern of both noble gases. This was already discussed by Bereiter, Shackleton, et al. (2018) but due to the simplicity of their box model they were unable to thoroughly assess its effect. We therefore test this in the Bern3D model by varying the extent of air-sea gas exchange allowed under sea-ice at the LGM, which is the simplest way to alter the saturation anomalies without impacting ocean physics and MOT. The model is only able to reproduce both reconstructed

$\delta\text{Kr}/\text{N}_2$ and $\delta\text{Xe}/\text{N}_2$ under the climate and ocean boundary conditions of the LGM control with saturation anomalies of -1.0% and -1.45% for Kr and Xe, respectively (or $+1.0\%$ and $+1.25\%$ relative to PI) (Figure 3b). Or in other words, only with these increases in saturation it is possible to derive the same ΔMOT from the two different reconstructed noble gas ratios. This observational constraint thus implies that the air-sea gas exchange in the Bern3D model is reduced too strongly at the LGM. The reason for this might be an overestimation of the glacial sea-ice extent, climate state dependent air-sea gas exchange under sea-ice (for instance due to the equatorward migration of sea-ice allowing for more leads to form), an underestimation of the wind induced change in gas transfer velocity due to the lack of a parameterization of bubble injection or the missing subsurface glacial melt-water addition. To explore the impacts of these processes and model biases future investigations are required to further bolster the assessment of past changes in noble gas saturation.

Therefore, leveraging both reconstructed atmospheric noble gas ratios and the Bern3D model, we conclude that the previous box model inferred ΔMOT is biased low by about $0.5 \pm 0.67^\circ\text{C}$ due to the assumption of constant noble gas undersaturation. Therefore, the model results suggest that the MOT was only around $2.1 \pm 0.71^\circ\text{C}$ colder during the LGM than PI, thus also reconciling reconstructions of ΔGMST and ΔGSST with the MOT anomaly.

4. Conclusions

We present a revised implementation of noble gases in the Bern3D model that we have tuned to observational constraints of modern saturation state. Through sensitivity tests we confirm that changing the undersaturation impacts the relationships between atmospheric noble gas ratios and MOT differently for Kr and Xe.

For the quasi-equilibrium state of the LGM we combine both, ice core measurements and the Bern3D model to better constrain the ocean's past noble gas saturation state and hence MOT. Together with theoretical considerations we find that the lower limit for the LGM MOT anomaly was -1.3°C assuming complete equilibration of noble gases at the air-sea interface. Yet, by gaining further constraints from small differences in the measured $\delta\text{Kr}/\text{N}_2$ and $\delta\text{Xe}/\text{N}_2$ derived MOT, we obtain a revised estimate for the past mean ocean saturation anomalies. This yields a best-estimate MOT anomaly of $-2.1 \pm 0.71^\circ\text{C}$ for the LGM in our model, which is about $0.5 \pm 0.67^\circ\text{C}$ warmer than previous noble gas derived estimates, and in improved agreement with independent ΔGMST and ΔGSST assessments. However, future experiments using other models are required to assess the model dependency of the size of this correction to the initially published ice core MOT values, and to more deeply explore the physical processes that drive the suggested LGM-PI change in inert gas saturation.

Data Availability Statement

Noble gas concentration data by Hamme et al. (2019) are publicly available at <https://www.bco-dmo.org/dataset/743867> (last access: 27. October 2022). Simulation outputs used in this study are available at <https://doi.org/10.5281/zenodo.7270250> (Pöppelmeier et al., 2022).

References

- Annan, J. D., & Hargreaves, J. C. (2013). A new global reconstruction of temperature changes at the Last Glacial Maximum. *Climate of the Past*, 9(1), 367–376. <https://doi.org/10.5194/cp-9-367-2013>
- Annan, J. D., Hargreaves, J. C., & Mauritsen, T. (2022). A new global reconstruction of temperature changes at the Last Glacial Maximum. *Climate of the Past*, 18(8), 1883–1896. <https://doi.org/10.5194/cp-18-1883-2022>
- Baggenstos, D., Häberli, M., Schmitt, J., Shackleton, S. A., Birner, B., Severinghaus, J. P., et al. (2019). Earth's radiative imbalance from the Last Glacial Maximum to the present. *Proceedings of the National Academy of Sciences of the United States of America*, 116(30), 14881–14886. <https://doi.org/10.1073/pnas.1905447116>
- Bereiter, B., Kawamura, K., & Severinghaus, J. P. (2018). New methods for measuring atmospheric heavy noble gas isotope and elemental ratios in ice core samples. *Rapid Communications in Mass Spectrometry*, 32(10), 801–814. <https://doi.org/10.1002/rcm.8099>
- Bereiter, B., Shackleton, S., Baggenstos, D., Kawamura, K., & Severinghaus, J. (2018). Mean global ocean temperatures during the last glacial transition. *Nature*, 553(7686), 39–44. <https://doi.org/10.1038/nature25152>
- Gleckler, P. J., Durack, P. J., Stouffer, R. J., Johnson, G. C., & Forest, C. E. (2016). Industrial-era global ocean heat uptake doubles in recent decades. *Nature Climate Change*, 6(4), 394–398. <https://doi.org/10.1038/nclimate2915>
- Häberli, M., Baggenstos, D., Schmitt, J., Grimmer, M., Michel, A., Kellerhals, T., & Fischer, H. (2021). Snapshots of mean ocean temperature over the last 700,000 yr using noble gases in the EPICA Dome C ice core. *Climate of the Past*, 17(2), 843–867. <https://doi.org/10.5194/cp-17-843-2021>
- Hamme, R. C., Emerson, S. R., Severinghaus, J. P., Long, M. C., & Yashayaev, I. (2017). Using noble gas measurements to derive air-sea process information and predict physical gas saturations. *Geophysical Research Letters*, 44(19), 9901–9909. <https://doi.org/10.1002/2017GL075123>

Acknowledgments

This study was supported by the European Union's Horizon 2020 research and innovation program under Grant 101023443 (project CliMoTran) to FP, No 820970 (project TiPES) to TFS. The work reflects only the authors' view; the European Commission and their executive agency are not responsible for any use that may be made of the information the work contains. TFS and HF are further supported by the Swiss National Science Foundation (Grants 200020_200492 and 200020_200328, respectively). Calculations were performed on UBELIX, the high-performance computing cluster at the University of Bern.

- Hamme, R. C., Nicholson, D. P., Jenkins, W. J., & Emerson, S. R. (2019). Using noble gases to assess the ocean's carbon pumps. *Annual Review of Marine Science*, 11(1), 75–103. <https://doi.org/10.1146/annurev-marine-121916-063604>
- Hamme, R. C., & Severinghaus, J. P. (2007). Trace gas disequilibria during deep-water formation. *Deep-Sea Research Part 1 Oceanographic Research Papers*, 54(6), 939–950. <https://doi.org/10.1016/j.dsr.2007.03.008>
- Headly, M. A., & Severinghaus, J. P. (2007). A method to measure Kr/N₂ ratios in air bubbles trapped in ice cores and its application in reconstructing past mean ocean temperature. *Journal of Geophysical Research*, 112(19), 1–12. <https://doi.org/10.1029/2006JD008317>
- Jenkins, W. J., Lott, D. E., & Cahill, K. L. (2019). A determination of atmospheric helium, neon, argon, krypton, and xenon solubility concentrations in water and seawater. *Marine Chemistry*, 211(March), 94–107. <https://doi.org/10.1016/j.marchem.2019.03.007>
- Kalnay, E., Kanamitsu, M., Kistler, R., Collins, W., Deaven, D., Gandin, L., et al. (1996). The NCEP NCAR 40-year reanalysis project. *Bulletin of the American Meteorological Society*, 77(3), 437–472. [https://doi.org/10.1175/1520-0477\(1996\)077<0437:TNYRP>2.0.CO;2](https://doi.org/10.1175/1520-0477(1996)077<0437:TNYRP>2.0.CO;2)
- Köhler, P., Nehrbass-Ahles, C., Schmitt, J., Stocker, T. F., & Fischer, H. (2017). A 156 kyr smoothed history of the atmospheric greenhouse gases CO₂, CH₄, and N₂O and their radiative forcing. *Earth System Science Data*, 9(1), 363–387. <https://doi.org/10.5194/essd-9-363-2017>
- Lambeck, K., Rouby, H., Purcell, A., Sun, Y., & Sambridge, M. (2014). Sea level and global ice volumes from the Last Glacial Maximum to the Holocene. *Proceedings of the National Academy of Sciences of the United States of America*, 111(43), 15296–15303. <https://doi.org/10.1073/pnas.1411762111>
- Loose, B., Jenkins, W. J., Moriaty, R., Brown, P., Jullion, L., Naveira Garabato, A. C., et al. (2016). Estimating the recharge properties of the deep ocean using noble gases and helium isotopes. *Journal of Geophysical Research: Oceans*, 121(8), 5959–5979. <https://doi.org/10.1002/2016JC01180>
- MARGO Project Members. (2009). Constraints on the magnitude and patterns of ocean cooling at the Last Glacial Maximum. *Nature Geoscience*, 2(2), 127–132. <https://doi.org/10.1038/ngeo411>
- Muglia, J., & Schmittner, A. (2015). Glacial Atlantic overturning increased by wind stress in climate models. *Geophysical Research Letters*, 42(22), 9862–9869. <https://doi.org/10.1002/2015GL064583>
- Müller, S. A., Joos, F., Edwards, N. R., & Stocker, T. F. (2006). Water mass distribution and ventilation time scales in a cost-efficient, three dimensional ocean model. *Journal of Climate*, 19(21), 5479–5499. <https://doi.org/10.1175/JCLI3911.1>
- Müller, S. A., Joos, F., Plattner, G. K., Edwards, N. R., & Stocker, T. F. (2008). Modeled natural and excess radiocarbon: Sensitivities to the gas exchange formulation and ocean transport strength. *Global Biogeochemical Cycles*, 22(3), 1–14. <https://doi.org/10.1029/2007GB003065>
- Osman, M. B., Tierney, J. E., Zhu, J., Tardif, R., Hakim, G. J., King, J., & Poulsen, C. J. (2021). Globally resolved surface temperatures since the Last Glacial Maximum. *Nature*, 599, 239–244. <https://doi.org/10.31223/XSS31Z>
- Pöppelmeier, F., Baggenstos, D., Grimmer, M., Liu, Z., Schmitt, J., Fischer, H., & Stocker, T. F. (2022). The effect of past saturation changes on noble gas reconstructions of mean ocean temperature: Model output data [Dataset]. Zenodo, <https://doi.org/10.5281/zenodo.7270250>
- Pöppelmeier, F., Scheen, J., Jeltsch-Thömmes, A., & Stocker, T. F. (2021). Simulated stability of the Atlantic meridional overturning circulation during the Last Glacial Maximum. *Climate of the Past*, 17(2), 615–632. <https://doi.org/10.5194/cp-17-615-2021>
- Ritz, S. P., Stocker, T. F., & Joos, F. (2011). A coupled dynamical ocean-energy balance atmosphere model for paleoclimate studies. *Journal of Climate*, 24(2), 349–375. <https://doi.org/10.1175/2010JCLI3351.1>
- Ritz, S. P., Stocker, T. F., & Severinghaus, J. P. (2011). Noble gases as proxies of mean ocean temperature: Sensitivity studies using a climate model of reduced complexity. *Quaternary Science Reviews*, 30(25–26), 3728–3741. <https://doi.org/10.1016/j.quascirev.2011.09.021>
- Seltzer, A. M., Pavia, F. J., Ng, J., & Severinghaus, J. P. (2019). Heavy noble gas isotopes as new constraints on the ventilation of the deep ocean. *Geophysical Research Letters*, 46(15), 8926–8932. <https://doi.org/10.1029/2019GL084089>
- Shackleton, S., Baggenstos, D., Menking, J. A., Dyonisius, M. N., Bereiter, B., Bauska, T. K., et al. (2020). Global ocean heat content in the Last Interglacial. *Nature Geoscience*, 13(1), 77–81. <https://doi.org/10.1038/s41561-019-0498-0>
- Shackleton, S., Bereiter, B., Baggenstos, D., Bauska, T. K., Brook, E. J., Marcott, S. A., & Severinghaus, J. P. (2019). Is the noble gas-based rate of ocean warming during the younger drys overestimated? *Geophysical Research Letters*, 46(11), 5928–5936. <https://doi.org/10.1029/2019GL082971>
- Shackleton, S., Menking, J. A., Brook, E., Buizert, C., Dyonisius, M. N., Petrenko, V. V., et al. (2021). Evolution of mean ocean temperature in marine isotope stage 4. *Climate of the Past*, 17(5), 2273–2289. <https://doi.org/10.5194/cp-17-2273-2021>
- Stocker, T. F. (2000). Past and future reorganizations in the climate system. *Quaternary Science Reviews*, 19(1–5), 301–319. [https://doi.org/10.1016/S0277-3791\(99\)00067-0](https://doi.org/10.1016/S0277-3791(99)00067-0)
- Tierney, J. E., Zhu, J., King, J., Malevich, S. B., Hakim, G. J., & Poulsen, C. J. (2020). Glacial cooling and climate sensitivity revisited. *Nature*, 584(7822), 569–573. <https://doi.org/10.1038/s41586-020-2617-x>

References From the Supporting Information

- Hamme, R. C., & Emerson, S. R. (2004). The solubility of neon, nitrogen and argon in distilled water and seawater. *Deep-Sea Research Part 1 Oceanographic Research Papers*, 51(11), 1517–1528. <https://doi.org/10.1016/j.dsr.2004.06.009>
- Weiss, R. F., & Kyser, T. K. (1978). Solubility of krypton in water and seawater. *Journal of Chemical and Engineering Data*, 23(1), 69–72. <https://doi.org/10.1021/je60076a014>

The effect of past saturation changes on noble gas reconstructions of mean ocean temperature

Frerk Pöppelmeier^{1,2*}, Daniel Baggenstos^{1,2,3}, Markus Grimmer^{1,2}, Zhijun Liu^{1,2,4}, Jochen Schmitt^{1,2}, Hubertus Fischer^{1,2}, Thomas F. Stocker^{1,2}

¹Climate and Environmental Physics, Physics Institute, University of Bern, Bern, Switzerland

²Oeschger Centre for Climate Change Research, University of Bern, Bern, Switzerland

³Australian Antarctic Division: Kingston, Tasmania, Australia

⁴GFZ German Research Centre for Geosciences, Potsdam, Germany

***Corresponding author:** Frerk Pöppelmeier (frerk.poeppelmeier@unibe.ch)

Contents of this file

Text S1

Tables S1

Figures S1 to S4

Text S1. Simplified 3-box model

We employ a simplified 3-box model similar to the 4-box model by Bereiter et al. (2018a), yet without an atmosphere and the important distinction that the input parameters directly correspond to quantities simulated in the Bern3D model, which are as such physically consistent. With this box model we are able to assess the theoretical noble gas atmospheric ratios in the absence of any undersaturation due to limited air-sea gas exchange. Further, we can directly compare these results with the ones derived from the 4-box model by Bereiter et al. (2018b). This is important because the mixing-induced oversaturation (see Hamme et al., 2019) is as such directly comparable, but underestimated in both box models compared to the Bern3D model, which encompasses far more realistic mixing schemes.

For the 3-box model we assume constant global noble gas inventories (atmosphere + ocean), which means that we can directly infer the atmosphere ratios from the mean ocean concentrations. We define the three boxes as northern-sourced water originating from the North Atlantic between 45-70°N (yellow dashed region in Fig. S1), southern-sourced water formed south of 45°S (blue dashed region), and the residual. The properties of these water masses (temperature and salinity) and their total volume fraction are derived from dye tracers in the Bern3D model that are set to 1 at the surface of the respective source region and are diluted elsewhere due to mixing with other water masses. Dissolved noble gas contents are calculated from the corresponding water mass properties after Jenkins et al. (2019). For the LGM the same corrections as for the Bern3D simulations (pressure and ocean volume) are applied to the box model (note that the temperature and salinity effects are directly considered by the inputs from the Bern3D model).

To determine the impact of changes in undersaturation on atmospheric $\delta\text{Kr}/\text{N}_2$ and $\delta\text{Xe}/\text{N}_2$ we compare the box model results with no changes in undersaturation to the changes in Bern3D where the undersaturation changes by 2.4% and 3.3% for Kr and Xe, respectively, in the pre-industrial radiative forcing experiments with a total change in MOT of 4.45 °C. As noted in the main text, the respective dependencies with MOT are $(\delta\text{Kr}/\text{N}_2)/\Delta\text{MOT} = 0.64 \text{ ‰}/^\circ\text{C}$ and $(\delta\text{Xe}/\text{N}_2)/\Delta\text{MOT} = 1.70 \text{ ‰}/^\circ\text{C}$ for the box model and $(\delta\text{Kr}/\text{N}_2)/\Delta\text{MOT} = 0.49 \text{ ‰}/^\circ\text{C}$ and $(\delta\text{Xe}/\text{N}_2)/\Delta\text{MOT} = 1.26 \text{ ‰}/^\circ\text{C}$ for Bern3D. It therefore follows for the change in atmospheric noble gas ratios with undersaturation:

$$\frac{\Delta(\delta\text{Kr}/\text{N}_2)}{\Delta\text{Sat}} = \left[(\delta\text{Kr}/\text{N}_2)/\text{MOT}(\text{Box}) - (\delta\text{Kr}/\text{N}_2)/\text{MOT}(\text{Bern3D}) \right] \cdot \frac{\Delta\text{MOT}}{\Delta\text{Sat}_{\text{tot}}} \quad (1)$$

with $\Delta\text{Sat}_{\text{tot}}$ the total change in Kr undersaturation over the 4.45 °C change in MOT in the Bern3D model radiative forcing experiments (i.e., 2.4%). For Xe the equivalent holds with $\Delta\text{Sat}_{\text{tot}} = 3.3\%$. In the main text we note the change

in atmospheric noble gas ratio ($\Delta\text{Kr}/\text{N}_2$ and $\Delta\text{Xe}/\text{N}_2$) per 1% change in global mean saturation anomaly (ΔSat).

Table S1: Difference between published data for the 4-box model by Bereiter et al. (2018) and revised calculations from this study.

	Bereiter et al. (2018)	This study
Solubility parameterization	Hamme & Emerson (2004); Weiss & Kyser (1978)	Jenkins et al. (2019)
Undersaturation	Monte-Carlo propagating of constant and 50% reduced undersaturation.	Constant
ΔMOT (LGM-Late Holocene)	-2.50 °C	-2.51 °C

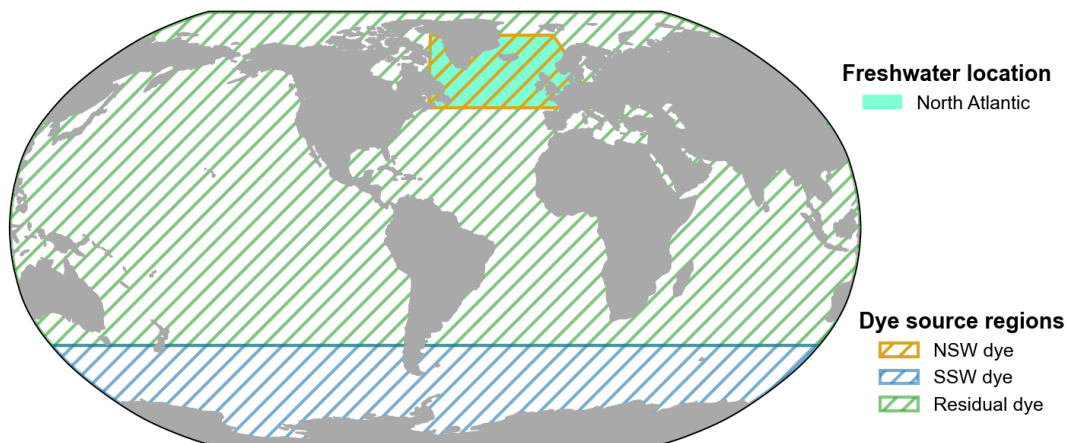


Figure S1. Global map with freshwater and dye tracer regions. Dashed regions indicate where the respective dye tracer concentrations are restored to 1 at the surface (i.e., the source regions of the dye tracers).

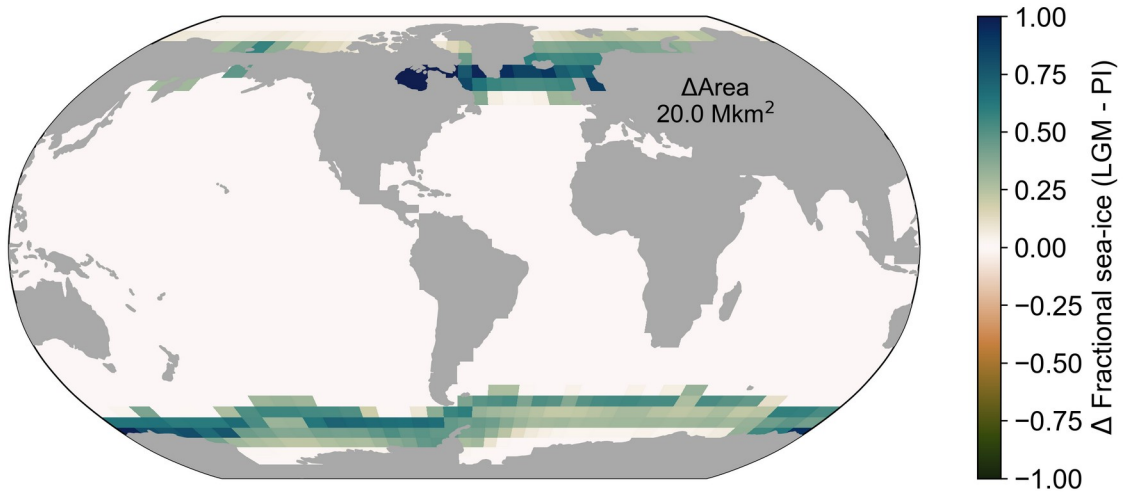


Figure S2. Difference in global fractional sea-ice extent between the LGM and PI control. Total difference in sea-ice area is 20 Mkm².

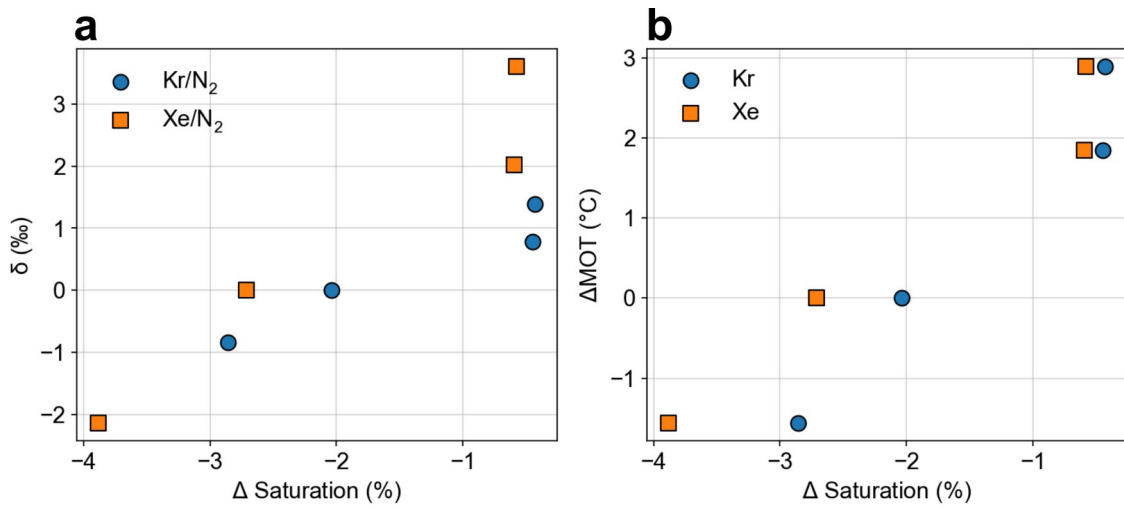


Figure S3. Cross plots of global mean saturation anomalies of Kr and Xe versus (a) atmospheric noble gas ratios, and (b) MOT anomalies (relative to the pre-industrial control) of the CO₂ sensitivity experiments.

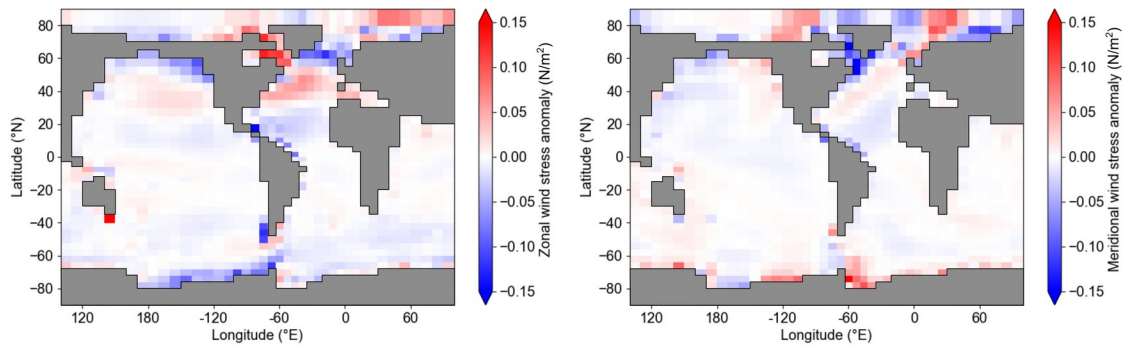


Figure S4. Multimodel mean wind stress anomalies of PMIP3 models following Muglia and Schmittner (2015). See Pöppelmeier et al. (2021) for details.

References

- Bereiter, B., Kawamura, K., & Severinghaus, J. P. (2018a). New methods for measuring atmospheric heavy noble gas isotope and elemental ratios in ice core samples. *Rapid Communications in Mass Spectrometry*, 32(10), 801-814. <https://doi.org/10.1002/rcm.8099>
- Bereiter, B., Shackleton, S., Baggenstos, D., Kawamura, K., & Severinghaus, J. (2018b). Mean global ocean temperatures during the last glacial transition. *Nature*, 553(7686), 39-44. <https://doi.org/10.1038/nature25152>
- Hamme, R. C., & Emerson, S. R. (2004). The solubility of neon, nitrogen and argon in distilled water and seawater. *Deep-Sea Research Part I: Oceanographic Research Papers*, 51(11), 1517-1528. <https://doi.org/10.1016/j.dsr.2004.06.009>
- Hamme, R. C., Nicholson, D. P., Jenkins, W. J., & Emerson, S. R. (2019). Using noble gases to assess the ocean's carbon pumps. *Annual Review of Marine Science*, 11, 75-103. <https://doi.org/10.1146/annurev-marine-121916-063604>
- Jenkins, W. J., Lott, D. E., & Cahill, K. L. (2019). A determination of atmospheric helium, neon, argon, krypton, and xenon solubility concentrations in water and seawater. *Marine Chemistry*, 211(March), 94-107. <https://doi.org/10.1016/j.marchem.2019.03.007>
- Muglia, J., & Schmittner, A. (2015). Glacial Atlantic overturning increased by wind stress in climate models. *Geophysical Research Letters*, 42(22), 9862-9869. <https://doi.org/10.1002/2015GL064583>
- Pöppelmeier, F., Scheen, J., Jeltsch-Thömmes, A., & Stocker, T. F. (2021). Simulated stability of the Atlantic Meridional Overturning Circulation during the Last Glacial Maximum. *Climate of the Past*, 17, 615-632. <https://doi.org/10.5194/cp-17-615-2021>
- Weiss, R. F., & Kyser, T. K. (1978). Solubility of Krypton in Water and Seawater. *Journal of Chemical and Engineering Data*, 23(1), 69-72. <https://doi.org/10.1021/je60076a014>